Proc. R. Soc. Lond. A. **364**, 1–28 (1978)
Printed in Great Britain

The deformation of steep surface waves on water

II. Growth of normal-mode instabilities†

By M. S. Longuet-Higgins‡ and E. D. Cokelet§

‡ *Department of Applied Mathematics and Theoretical Physics, Silver Street, Cambridge, U.K.*

‡§ *Institute of Oceanographic Sciences, Wormley, Surrey, U.K.*

(*Received* 3 *April* 1978)

Studies of the normal-mode perturbations of steep gravity waves (Longuet-Higgins 1978 *b*, *c*) have suggested two distinct types of instability: at low wave steepnesses we find subharmonic instabilities with fairly low rates of growth, and at higher wave steepnesses there are apparently local ('superharmonic') instabilities leading directly to wave breaking. Between these two types of instability is an intermediate range of wave steepnesses where the unperturbed wave train is neutrally stable.

In the present paper we employ the time-stepping method of an earlier paper (Longuet-Higgins & Cokelet 1976) to test the rate of growth of each type of instability. For the initial linear stages of each instability, the computed rates of growth are accurately confirmed, and it is verified that the local instability does indeed lead to breaking.

The later nonlinear stages of the subharmonic instabilities are further investigated. In the two examples so far computed it is found that the gradual rates of growth of the subharmonic instabilities are maintained, and that ultimately every alternate crest develops a fast-growing local instability which quickly leads to breaking.

1. Introduction

The task of understanding and predicting the formation of breaking waves on deep water has recently been approached in two different ways. On the one hand a general method has been developed for calculating the deformation of the free surface in any irrotational motion which is periodic in the horizontal coordinate (Longuet-Higgins & Cokelet 1976; referred to as paper I). This has been applied successfully to a variety of initial conditions (see I and also Cokelet 1977). On the other hand a more analytical approach (Longuet-Higgins 1978 *b*, *c*) has yielded some understanding of the initial rates of growth of any small perturbations to a uniform train of waves of finite amplitude.

The conclusions reached in the more recent papers (Longuet-Higgins 1978 *b*, *c*) were somewhat surprising. For instance it was found that there were at least two distinct types of instability: subharmonic instabilities of the Benjamin–Feir type,

† Part I appeared in *Proc. R. Soc. Lond.* A **350**, 1–26.

which were however confined to waves whose 'steepness' ak lay within a certain finite range (the upper limit being at $ak \approx 0.37$ and the maximum growth-rate at $ak \approx 0.32$); and secondly, local or superharmonic instabilities which first appeared when $ak \approx 0.41$. These had much higher rates of growth, and it was suggested that they led directly to overturning of the free surface, that is to say breaking waves.

With regard to the subharmonic instabilities, rather good confirmation of the calculated growth rates was provided by the observations reported by Benjamin (1967). But these were only for small values of the wave steepness ($ak < 0.17$). At higher values of ak no direct measurements are yet available.

The calculations reported by Longuet-Higgins (1978*b*, *c*) were lengthy. Because of the need to verify the somewhat unexpected conclusions relating to instabilities at higher values of ak, the present authors have, in this paper, set out to determine the initial growth-rates of each type of instability by the quite independent time-stepping method of paper I. This method is indeed well suited to the present problem whenever the initial perturbation has a length-scale equal to an integral number m of wavelengths of the unperturbed wave. Here we concentrate particularly on the case $m = 2$ when the perturbations are two wavelengths long. This case has the advantage that the numerical calculations are the most accurate for any value of m at the higher values of ak, where confirmation is most needed. Also, they display all the unexpected features mentioned earlier.

These features are set out in more detail in §2. In §3 we briefly describe the time-stepping method, to be applied in the present instance. Sections 4 and 5 describe the main results as they relate to the initial rates of growth. From table 1 and figure 5 it will be seen that the agreement between the two methods is remarkably good.

But the time-stepping method used in the present paper has the further advantage that (unlike perturbation analysis) its validity is not limited to *small* perturbations of the finite-amplitude wave. Being without analytic approximation, the numerical calculation can be carried to the point when the perturbations themselves are of finite amplitude. This is done in §§ 6 and 7. As a result it is found, first, that the 'local' instabilities do indeed lead directly to wave breaking, in which the final overturning takes place very rapidly (figures 15 and 18). Secondly, the subharmonic instabilities, when followed to their later stages of growth, develop local instabilities at every alternate wave crest. These local instabilities are precisely similar to the local instabilities found previously. In other words, the disintegration of the wave train, which is brought about by the subharmonic instabilities, extends as far as to make the waves break, in all those cases that we have tried. Moreover, the computed behaviour of the wave crests is so similar in all cases that there is hope for a local, asymptotic theory of the dynamics.

Finally we should like to emphasize that, unlike those in paper I, the waves treated here are theoretically free waves, with constant and uniform pressure at the free surface. Thus there is no input of energy; we are studying the dynamics of breaking waves under the simplest possible conditions.

2. The normal-mode analysis

In the perturbation analysis of Longuet-Higgins (1978*b*, *c*) the normal modes were calculated in the form

$$\left.\begin{aligned} x &= X(\phi,\psi)+\epsilon\hat{\xi}(\phi,\psi)\,\mathrm{e}^{-\mathrm{i}\sigma t},\\ y &= Y(\phi,\psi)+\epsilon\hat{\eta}(\phi,\psi)\,\mathrm{e}^{-\mathrm{i}\sigma t},\end{aligned}\right\} \tag{2.1}$$

where ϕ and ψ denote the velocity potential and stream function in a frame of reference moving with the speed c of the unperturbed wave, and x, y are rectangular coordinates (x horizontal, y vertically upwards) expressed in terms of ϕ, ψ and the time t as independent variables. X and Y represent the coordinates of the unperturbed wave, and $\hat{\xi}$, $\hat{\eta}$ the normalized perturbation, ϵ being an arbitrary small parameter. The free surface, which in the unperturbed wave is given by $\psi = 0$, is given by

$$\psi = \epsilon\hat{f}(\phi)\,\mathrm{e}^{-\mathrm{i}\sigma t} \tag{2.2}$$

in the perturbed state. In fact $\hat{\xi}$, $\hat{\eta}$ and $\hat{f}$ have both real and imaginary parts, corresponding to the 'in-phase' and 'quadrature' components of the normal mode, and each of these components is given, in turn, by Fourier series in $\cos(l\phi/c)$ and in $\sin(l\phi/c)$, where l is a non-negative integer and ϕ runs from 0 to $2m\pi/c$.

Throughout this paper the units of length and time are normalized by taking $g = 1$ and the wavelength of the unperturbed wave to be 2π.

It was shown by Longuet-Higgins (1978*b*, *c*) that each normal mode may be designated by one or more rational numbers (mode numbers) which indicate its principal wavenumber components when ak is small. For example $n = (\frac{1}{2}, \frac{3}{2})$ denotes a subharmonic normal mode with principal components having wavenumbers $\frac{1}{2}$ and $\frac{3}{2}$. An index $+$ or $-$ may be added to designate that the perturbation is either growing or decaying, respectively.

In general σ is a complex quantity, and the frequencies occur in conjugate pairs. The unstable modes are those for which σ has a positive imaginary part. The calculations revealed two distinct types of instability. The first are *sub*harmonics, with wavelengths greater than that of the unperturbed wave. At small wave steepness ak these are clearly of the Benjamin–Feir type (Benjamin 1967). If we imagine the side-band frequency $\Delta\sigma$ as fixed and the steepness ak of the unperturbed wave to increase gradually, then these subharmonic modes first become unstable when ak slightly exceeds $\Delta\sigma/\surd 2$. The maximum rate of growth is found for a normal perturbation two wavelengths long, at an amplitude $ak \approx 0.32$. But when ak slightly exceeds 0.37 the perturbation apparently becomes neutrally stable again: the instability disappears (a result first predicted by Lighthill (1967)). Beyond $ak = 0.37$ the normal-mode analysis of Longuet-Higgins (1978*c*) indicates a narrow range of neutral stability, culminating in the onset of a second type of instability which (it was suggested) is more local, being concentrated near the crests of individual waves. For this type, σ is pure imaginary, and the initial rate of growth is much higher. It was foreseen that these instabilities might develop directly into breaking waves.

3. The time-stepping method

In the present paper we aim to test and extend these results by the entirely independent time-stepping method developed in I. This method is based on the fact that in an irrotational, incompressible fluid the kinematic and dynamic boundary conditions describe the evolution of the flow in terms of quantities specified only on the boundaries. For deep-water waves, the only boundary is the free surface, the region of greatest interest. Its location is given by the coordinates, (x_j^*, y_j^*), $j = 1, 2, \ldots, N$, of specified fluid particles. In order to follow the motions of the surface we need know only the tangential and normal velocities of the particles on it. Given the value of the velocity potential ϕ^* along the surface we find the tangential velocity $\partial\phi^*/\partial s$ by numerical differentiation. To find the normal velocity $\partial\phi^*/\partial n$ we use Green's third identity ((4.2) of paper I) to derive an integral equation for $\partial\phi^*/\partial n$ in terms of other surface-evaluated quantities. Having solved this equation numerically we march forward in time with the evolution equations ((2.7) and (2.10) of paper I).

The motion is assumed to be periodic in the horizontal coordinate, though not necessarily in the time t. This assumption enables us to transform the semi-infinite region of fluid (x^*, y^*-plane) into a finite enclosed region (ζ-plane) such that the free surface maps to the exterior boundary (see § 3 of I). The basic numerical computations are performed in this transformed plane.

Evidently the time-stepping method can be adapted without essential change to the present problem, provided the spatial period L contains m wavelengths of the unperturbed motion (m an integer). In the present paper we confine ourselves to the case $m = 2$, first because the initial perturbations, as calculated by the normal-mode method (Longuet-Higgins 1978*b*, *c*), are given most accurately when $m = 1$ or 2, at the larger values of ak. Secondly, the case $m = 1$ excludes *sub*harmonic instabilities and yields only the localized instabilities; and these occur at slightly higher values of ak than when $m = 2$ so the accuracy is correspondingly less. By considering $m = 2$ we shall include both types of instability, and with greater initial accuracy.

A third advantage of the case $m = 2$ is that, of all integer values of m, this yields the subharmonic instability having the highest growth-rate, namely when

$$n = (\tfrac{1}{2}, \tfrac{3}{2}), \quad ak = 0.32.$$

In the time-stepping method the reference frame is stationary, relative to the water at infinite depth. So if we denote the velocity-potential and stream-function by ϕ^*, ψ^*, and the rectangular coordinates by x^*, y^*, we have the relations†

$$\left.\begin{aligned} x^* &= x + ct, & \phi^* &= \phi + cx^*, \\ y^* &= y, & \psi^* &= \psi + cy^*. \end{aligned}\right\} \tag{3.1}$$

† In (Longuet-Higgins 1978*b*, *c*) the undisturbed waves were taken to be propagating in the negative x-direction. Here we assume they propagate in the positive sense.

To begin the time-stepping we need only to know the values of x^*, y^* and ϕ^* when $\psi = \epsilon\hat{f}$, as a function of some parameter which increases monotonically along the free surface. (Here one can take this to be ϕ/c in the first place.) Now on the free surface $\psi = \epsilon\hat{f}$ we have from (2.1) to first order,

$$\left.\begin{aligned} x &= X(\phi,0)+\epsilon\hat{f}(\phi)\,X_\psi(\phi,0)+\epsilon\hat{\xi}(\phi,0),\\ y &= Y(\phi,0)+\epsilon\hat{f}(\phi)\,Y_\psi(\phi,0)+\epsilon\hat{\eta}(\phi,0),\end{aligned}\right\} \tag{3.2}$$

when $t = 0$; and it remains now only to write

$$x^* = x, \quad y^* = y, \quad \phi^* = \phi + cx, \tag{3.3}$$

where x and y are given by (3.2).

The computation points were at first taken at N equally spaced values of ϕ along the free surface. Later it was found that improved accuracy could be obtained by distributing the points at equally spaced intervals of arc length in the transformed ζ-plane (see I, § 3). Normally N was taken as 90 but occasionally 60 or 120 according to the accuracy required. After the initial distribution, the same points were followed as Lagrangian marker points throughout the rest of the computation. This proved beneficial because they tended to concentrate at the crests, the regions of largest curvature.

The computations were programmed in FORTRAN IV and performed on Rutherford High Energy Laboratory's IBM 360/195 digital computer. The array storage requirements were proportional to (N^2+77N) and in double precision (8 bytes/word) the core storage (arrays + buffers + system overheads) was 310 K bytes (1 K = 1024) for $N = 90$. The computations were first limited by the availability and expense of computer time. With $N = 90$ the time required (*ca.* N^2) for one solution of the integral equation (4.5) of I was 2.2 s. This usually had to be solved twice per time-step when Adams–Bashforth–Moulton time-stepping was used. The time-step Δt was adjusted so that no particle moved further in a time-step than the distance between itself and an adjacent particle. When Δt was altered, three Runge–Kutta steps requiring four solutions of the integral equation were taken. The amount of computer time per run varied a great deal, but generally higher waves took longer because of large particle velocities and hence smaller time-steps. In the examples to be described, the runs typically required 5–10 min of machine time.

Throughout the computation, the surface pressure was assumed to be zero.

4. Example

Now as an example of the time-stepping computation described in § 3 we show in figure 1 the results of a computation for the perturbation $n = (\frac{1}{2}, \frac{3}{2})^+$ when $ak = 0.32$. According to the normal-mode calculations (Longuet-Higgins 1978*b*, *c*) this should in fact be the fastest-growing mode of the Benjamin–Feir type. In the left hand column of figure 1 are shown two successive crests of the perturbed wave, with time increasing down the page. At the top right is shown the initial perturbation, according to equation (2.3) but with the vertical scale multiplied by a factor 5, for clarity. Below this, corresponding to each profile on the left, is the perturbation calculated by taking the difference between the profile on the left and the unperturbed wave advanced with the theoretical phase-speed c.

It will be noticed, first, that every alternate crest of the original profile is higher, in general, and the intermediate crests are lower. This is because the perturbation is an *odd* one, being equal, but of opposite sign, on adjacent crests.

Next it will be seen that after half a cycle of the perturbation (namely at the foot of figure 1) the waves that were the higher have become lower, and vice versa.

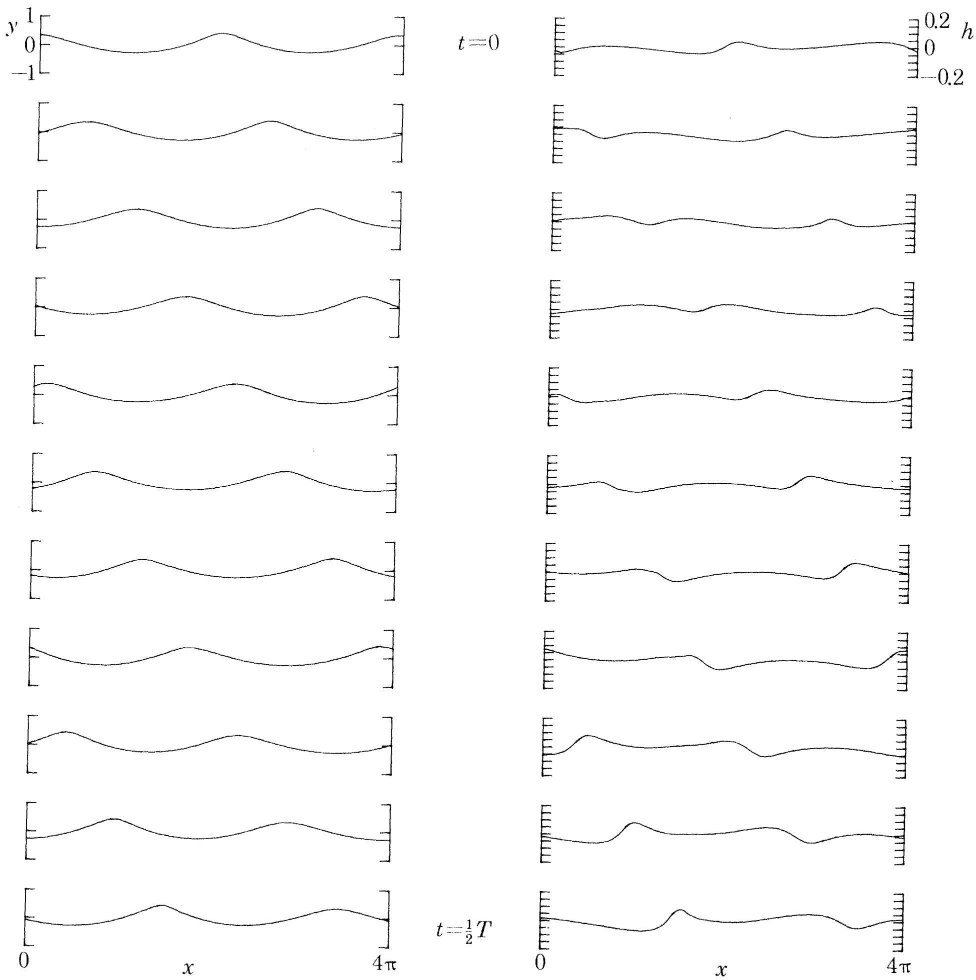

FIGURE 1. Development of the subharmonic instability $(\frac{1}{2}, \frac{3}{2})^+$ over one half-period of the perturbation, when $ak = 0.32$. The left hand column shows the time-stepped surface profiles. The right hand column shows the resulting perturbation, enlarged vertically by a factor 5. Time increases downwards. In this case $N = 90$, $\epsilon = 0.025$.

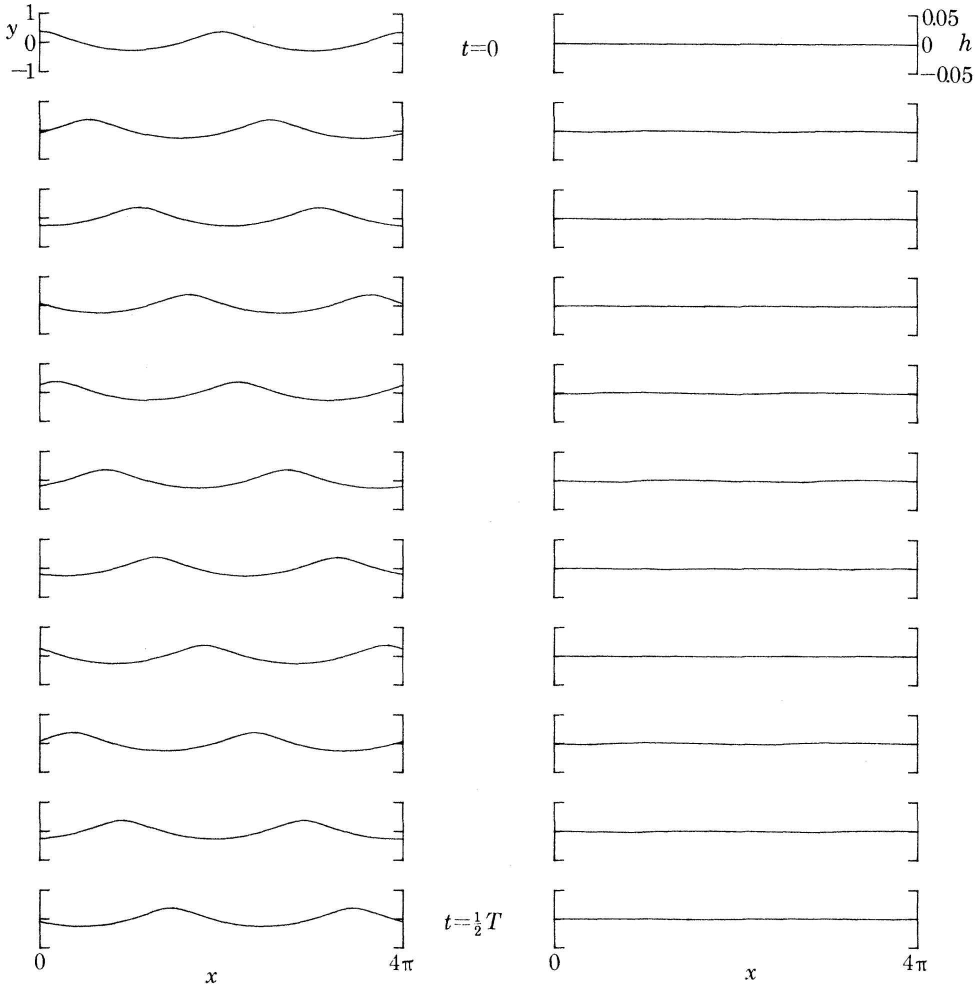

FIGURE 2. As in figure 1, but with $\epsilon = 0$ (zero perturbation). This tests the accuracy of the time-stepping technique. On the right, the vertical scale is enlarged times 20.

This is because after a half-cycle the perturbation is exactly proportional to its initial value, but of opposite sign.

Third it will be seen, by comparing the perturbations at the top and bottom of figure 1, that the magnitude of the perturbation has indeed increased.

Figure 2 shows a precisely similar computation but with $\epsilon = 0$, that is, the initial perturbation is zero. This is simply a test of the accuracy of the time-stepping. After the same interval of time the perturbation shown on the right (magn. $\times 20$) has in fact grown very little; it is a measure of the error inherent in the calculation. The r.m.s. amplitude of the perturbation was less than 4×10^{-4}.

Now figure 3 shows the companion mode $n = (\frac{1}{2}, \frac{3}{2})^-$ which is expected to decay. Again, comparison of the perturbations at top and bottom of the figure shows that the perturbation is indeed diminished.

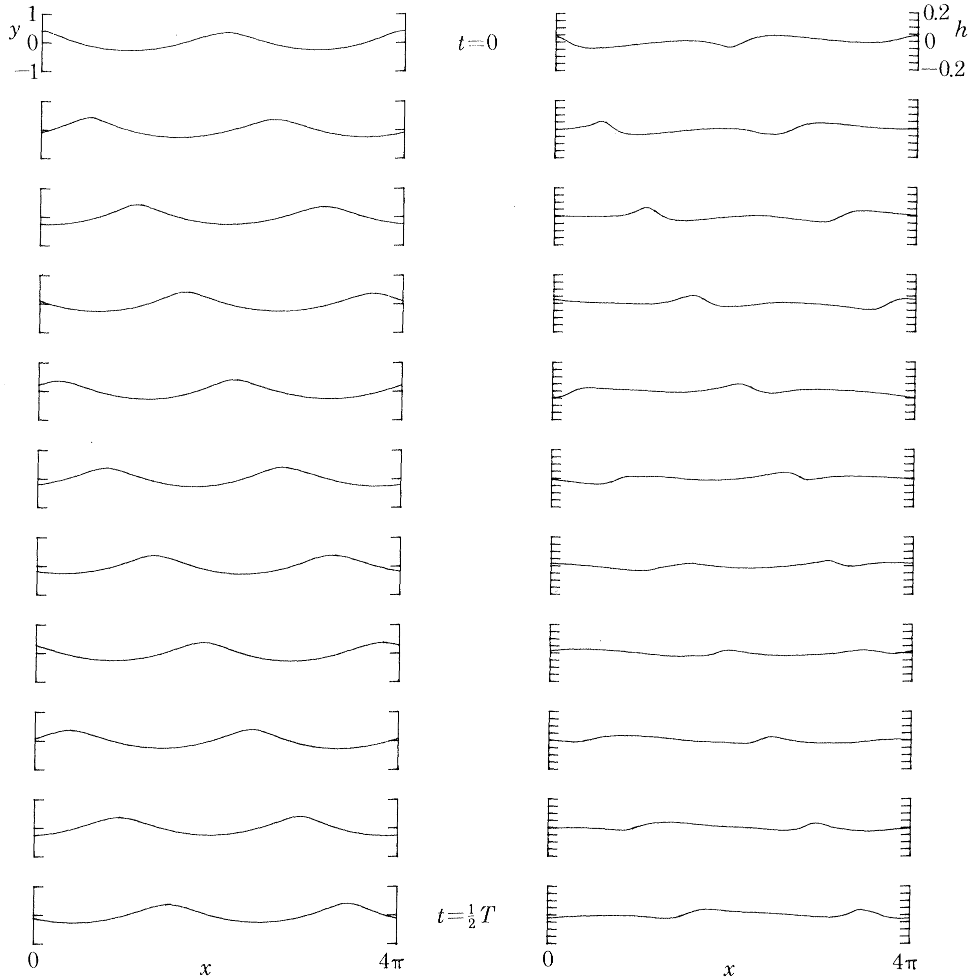

FIGURE 3. Development of the decaying mode $(\frac{1}{2}, \frac{3}{2})^-$ when $ak = 0.32$. Parameters as in figure 1.

5. Calculation of the growth rate

To determine the rate of growth of the perturbation $h(x^*, t)$ over a given interval of time, say $(0, t)$, we aim to determine the ratio $R(t)$ of the root-mean-square values of $h(x^*, t)$ and $h(x^*, 0)$. By definition†

$$\{R(t)\}^2 = \int_0^{4\pi} \{h(x, t)\}^2 \, \mathrm{d}x \bigg/ \int_0^{4\pi} \{h(x, 0)\}^2 \, \mathrm{d}x. \tag{5.1}$$

It is also useful to define the correlation coefficient between $h(x, t)$ and $h(x + x_0, 0)$ by

$$C(x_0, t) = \frac{\int h(x, t)\, h(x + x_0, 0) \, \mathrm{d}x}{[\int \{h(x, t)\}^2 \, \mathrm{d}x \int \{h(x + x_0, 0)\}^2 \, \mathrm{d}x]^{\frac{1}{2}}}. \tag{5.2}$$

† In this section x and y are written for x^* and y^*. This should cause no confusion with the notation of § 2.

We might expect the maximum correlation between $h(x,t)$ and $h(x+x_0, 0)$ when $x_0 = ct$, where c is the phase velocity. However, since $\hat{\eta}\,e^{-i\sigma t}$ has both a real and an imaginary part, corresponding to components in-phase and in quadrature with the initial perturbation, the maximum (absolute) correlation will in general fluctuate in time. If T denotes the period of the perturbation ($T = 2\pi/\mathrm{Re}\,(\sigma)$) then at times $t = sT$, where s is an integer, we should expect $C(ct,t)$ to be near unity; while at times $t = (s+\frac{1}{2})\,T$ we should expect $C(ct,t)$ to be nearly -1. Provided the maximum value of $|C(x_0,t)|$ is near unity, then a useful measure of the growth-rate should be derived from the corresponding value of $R(t)$. In fact we would expect that while the perturbation is still small

$$R(t) \approx e^{\beta t}, \quad \beta = \mathrm{Im}\,(\sigma). \tag{5.3}$$

The actual determination of the integrals in (5.1) and (5.2) must be done with care. The computer program begins at $t = 0$, and has its own method of determining the time-step length, Δt. In general the flow will not be computed at exactly $t = \frac{1}{2}sT$, but rather at times before and after this. Hence it is necessary to interpolate the particle positions to this time. This can be done in a variety of ways. Let us assume we have a simple equation of the form

$$\mathrm{d}y/\mathrm{d}t = f(t), \tag{5.4}$$

and we store y and f at every time-step. Our time-stepping technique is fourth-order (local errors $\sim (\Delta t)^5$) which means it would be consistent to use five pieces of information about y and f for interpolation. However it seems a good idea to use information only at times t_1 and t_2 which bracket the time of interest, t. This implies a cubic interpolation formula (errors $\sim (\Delta t)^4$) based on y_1, y_2, f_1 and f_2 (here subscripts denote time levels). We tried interpolating the particle positions using such a formula, and it was clear that the results were 'noisy'. A linear interpolation (errors $\sim (\Delta t)^2$) based on just the particle positions themselves was much smoother. This is to be expected since the displacements are calculated from the time derivatives by integration, a smoothing process. In order to have a smooth interpolant $\bar{y}(t)$, and to make use of both the displacement and derivative information at t_1 and t_2, we took the average of two quadratics each fitted through t_1 and t_2 but with one using f_1 and the other using f_2. Thus we have

$$\bar{y}(t) = At^2 + Bt + D, \tag{5.5}$$

where

$$\left.\begin{aligned} A &= \frac{f_2-f_1}{2\Delta t}, \\ B &= \frac{f_1+f_2}{2} + \frac{y_2-y_1}{\Delta t} + \frac{t_1 f_1 - t_2 f_2}{\Delta t}, \\ D &= \frac{y_1+y_2}{2} - \tfrac{1}{2}A(t_1^2+t_2^2) - \tfrac{1}{2}B(t_1+t_2). \end{aligned}\right\} \tag{5.6}$$

This interpolation formula is exact for quadratics and has local errors which vary as $(\Delta t)^3$.

Once the positions of the fluid particles are interpolated to the required time we wish to determine the shape of the perturbation. The free surface is specified by

$$y = H(x,t)+h(x,t), \tag{5.7}$$

where H represents the contribution from an unperturbed steady wave and h represents the perturbation. The steady wave profile is calculated by the technique of Longuet-Higgins (1978*a*) at $t = 0$, and for some later time it is just horizontally displaced by an amount ct where c is its phase speed. The perturbed wave profile is represented by the collection of points (x_j, y_j), $j = 1, \ldots, N$ and to calculate $h_j = h(x_j, t)$ we simply subtract $H_j = H(x_j, t)$ from y_j. However in practice we represent $H(x,t)$ by another collection of N points, and the horizontal coordinates of these will not necessarily coincide with the x_j. Therefore we use a periodic cubic spline to interpolate $H(x,t)$ in space.

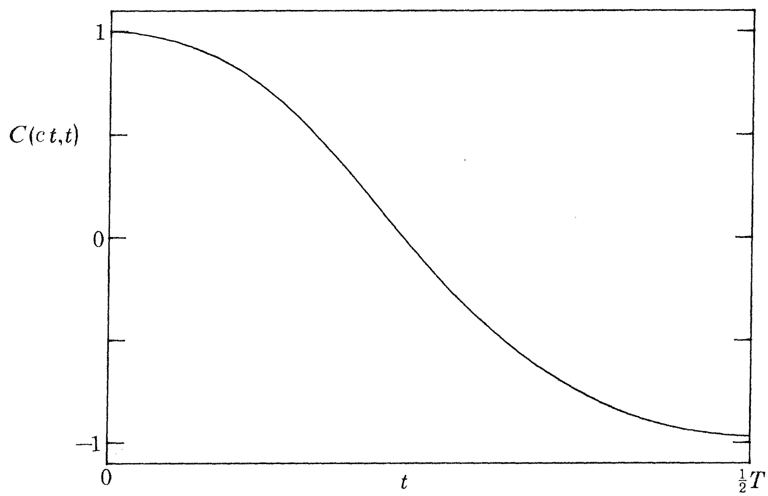

FIGURE 4. The correlation coefficient $C(ct, t)$ between $h(x, t)$ and $h(x+ct, 0)$ as a function of the time t for the perturbation $(\frac{1}{2}, \frac{3}{2})^+$ when $ak = 0.32$ (see figure 1).

We calculated the integrals in (5.1) and (5.2) by interpolating $h(x,t)$ to equally spaced values of x with periodic cubic splines, and then using the Simpson rule. The value of $C(ct,t)$ is plotted in figure 4 as a function of the time t, for the particular mode $n = (\frac{1}{2}, \frac{3}{2})^+$ discussed in § 4. It can be seen that $C(ct,t)$ does indeed fluctuate in time, with extrema at about $t = \frac{1}{2}sT$ $(s = 0, 1, 2, \ldots)$ as expected.

Of particular interest is the value of $R(t)$ at $t = \frac{1}{2}sT$ $(s = 1, 2, 3, \ldots)$ and the corresponding rate of growth

$$\beta' = t^{-1} \ln R(t).$$

For $ak = 0.32$, $n = (\frac{1}{2}, \frac{3}{2})^+$ we find that, when $t = \frac{1}{2}T$ then $\beta' = 0.0254$ and when $t = T$, then $\beta' = 0.0254$. This is to be compared with the value $\beta = 0.0234$ obtained by the normal-mode analysis (see table 1).

TABLE 1. COMPARISON OF CALCULATED GROWTH-RATES OF NORMAL-MODE PERTURBATIONS

			normal-mode calculation			time-stepping with integral equation		
ak	$c(k/g)^{\frac{1}{2}}$	n	α Re (σ)	$\frac{1}{2}T$ (π/α)	β Im (σ)	$C(ct, t)$	$R(t)$	β' $t^{-1}\ln R$
0.10	1.005013	$\frac{1}{2}$	.2072	15.17	.0000	−.999	0.999	−.0001
		$\frac{3}{2}$	.2676	11.74	.0000	−.997	0.995	−.0004
0.20	1.020203	$\frac{1}{2}$	.2098	14.97	.0000	−.996	1.002	.0001
		$\frac{3}{2}$	.2406	13.06	.0000	−.990	1.000	.0000
0.25	1.031746	$(\frac{1}{2}, \frac{3}{2})^+$	.2150	14.61	.0132	−.992	1.219	.0135
		$(\frac{1}{2}, \frac{3}{2})^-$	.2150	14.61	−.0132	−.980	0.833	−.0125
0.32	1.052512	$(\frac{1}{2}, \frac{3}{2})^+$	.1931	16.27	.0234	−.969	1.512	.0254
		$(\frac{1}{2}, \frac{3}{2})^-$	.1931	16.27	−.0234	−.786	0.752	−.0175
0.38	1.074399	$\frac{1}{2}$	.1804	17.41	.0000	−.994	0.985	−.0009
		$\frac{3}{2}$	.1309	24.00	.0000	−.853	0.909	−.0040
0.40	1.082225	$\frac{1}{2}$	.1840	17.07	.0000	−.908	1.118	.0065
0.41	1.086045	$(\frac{3}{2})^+$	.0000	∞	.065	—	—	—

6. RESULTS

Similar calculations were carried out for the modes $n = (\frac{1}{2}, \frac{3}{2})$ at the unperturbed wave amplitudes $ak = 0.10$, 0.20, 0.25, 0.32, 0.38, 0.40 and 0.41. For the normal modes under consideration the perturbation theory (Longuet-Higgins 1978*c*) predicts that at the two lowest values of ak the waves will be stable, at the next two they will be unstable, at the next two they will be stable again, and at the highest value of ak they will be violently unstable. This general behaviour is confirmed by our computations. Figure 5 shows a graph of the growth-rate β plotted against the unperturbed wave amplitude ak. The solid curve represents the growth-rates according to Longuet-Higgins (1978*b*), and the points represent the present results. The surprising prediction of a return to stability with increasing wave amplitude is confirmed reasonably well. Departures of the observed growth-rates from the predicted ones are probably due to computational inaccuracies, although the finite amplitude of the perturbation may play a rôle. The results for the highly unstable mode at $ak = 0.41$ are not shown on figure 5 but will be discussed later. In all cases except $ak = 0.32$ we took $\epsilon = 0.0125$.

Table 1 lists the quantitative results of the calculations. The first six columns give the unperturbed wave amplitude and phase speed, the mode of the perturbation, its frequency in a reference frame moving with the unperturbed wave, the semi-period of the perturbation and the growth-rate. These quantities are all derived from the normal-mode theory. The last three columns give the maximum correlation coefficient, the r.m.s. amplitude ratio and the observed growth-rate, all evaluated at $t = \frac{1}{2}T$. We shall now discuss the results in detail beginning with the lowest waves.

At $ak = 0.10$, the modes $n = \frac{1}{2}$ and $n = \frac{3}{2}$ display a negligible growth-rate, as shown in the last column of table 1. The correlation coefficients are -0.999 and -0.997 respectively, after one semi-period. These imply very little change of shape, and this is verified by an inspection of the profiles in figures 6 and 7. On the left of each figure are the complete wave profiles, plotted every one tenth of a semi-period. The reference frame is at rest, i.e. the average horizontal fluid velocity is zero at any point which lies always below the free surface. The perturbation profiles $h(x, t)$, plotted with a vertical exaggeration of 20:1, are on the right. Note how in figure 6 the smooth profile of h is very nearly a sine wave of length 4π. This

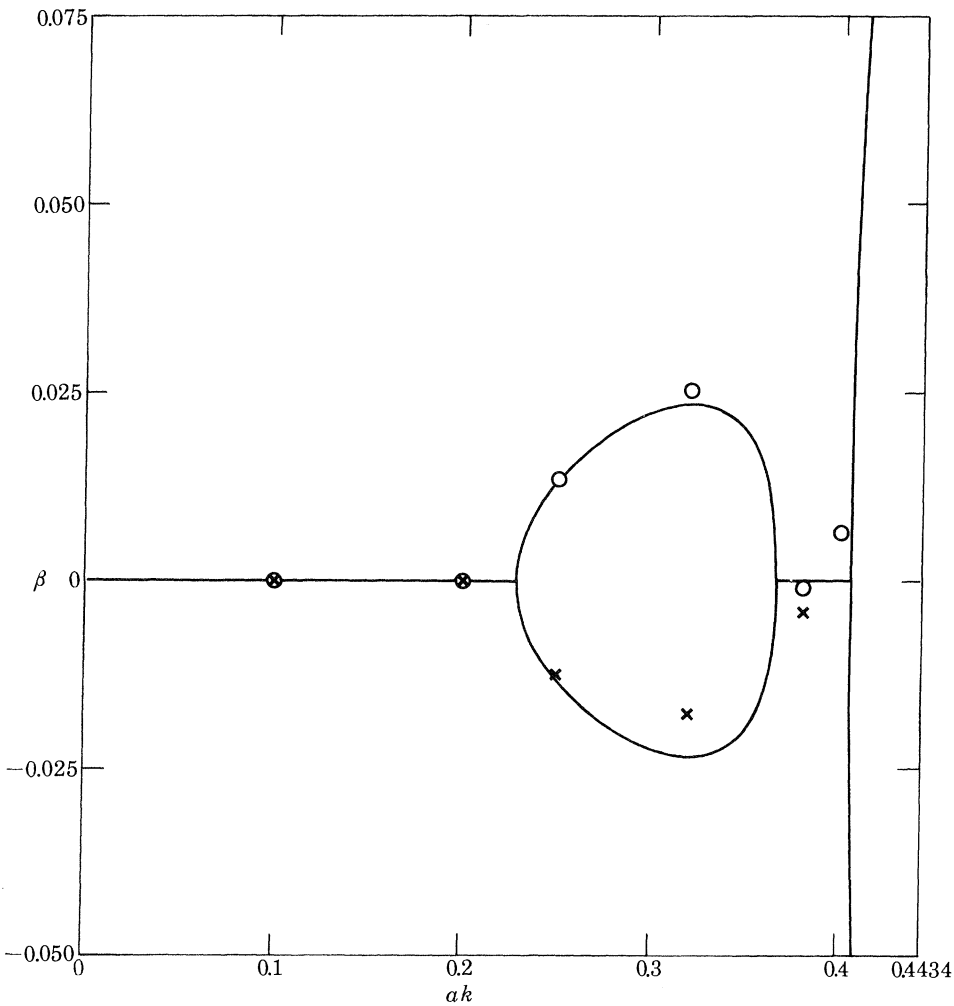

FIGURE 5. The linear growth-rate β of the normal perturbations $n = \frac{1}{2}, \frac{3}{2}$ and $(\frac{1}{2}, \frac{3}{2})^{\pm}$ as a function of the steepness ak of the unperturbed wave train. Curves represent the normal-mode calculations of Longuet-Higgins (1978*b*). Plotted points are from the time-stepping method of the present paper. ○, $n = \frac{1}{2}$ and $(\frac{1}{2}, \frac{3}{2})^{+}$; ×, $n = \frac{3}{2}$ and $(\frac{1}{2}, \frac{3}{2})^{-}$.

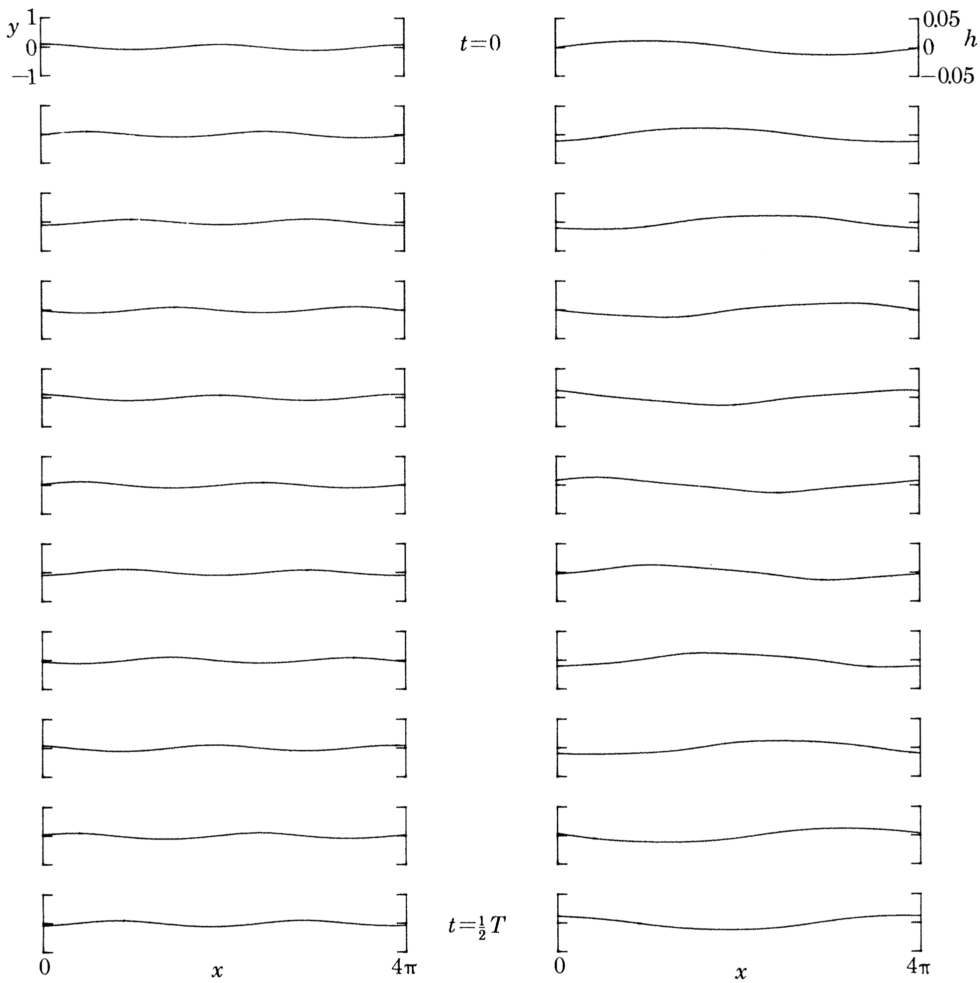

FIGURE 6. The mode $n = \frac{1}{2}$ when $ak = 0.10$ followed over one half-cycle of the perturbation. The left hand column shows the time-stepped profiles. The right hand column shows the resulting perturbation enlarged vertically by a factor 20. Time increases downwards. $\epsilon = 0.0125$.

is to be expected since this mode is exactly a sine wave in the limit as $ak \to 0$ (which is the basis for the notation $n = \frac{1}{2}$, signifying one sine wave in two fundamental wavelengths). Likewise the profile of the mode $n = \frac{3}{2}$ in figure 7 is predominantly three sine waves.

The profiles for $ak = 0.20$, $n = \frac{1}{2}$ and $\frac{3}{2}$ are illustrated in figures 8 and 9. Comparing these to figures 6 and 7 we see that the increased nonlinearity of the unperturbed waves enhances the higher harmonic content of the perturbation profiles, local bumps and dips begin to appear. The correlation coefficients are -0.996 and -0.990, and the growth-rates are 0.0001 and 0.0000 for $n = \frac{1}{2}$ and $\frac{3}{2}$ respectively. This extremely good agreement with theory is heartening when it is realized that

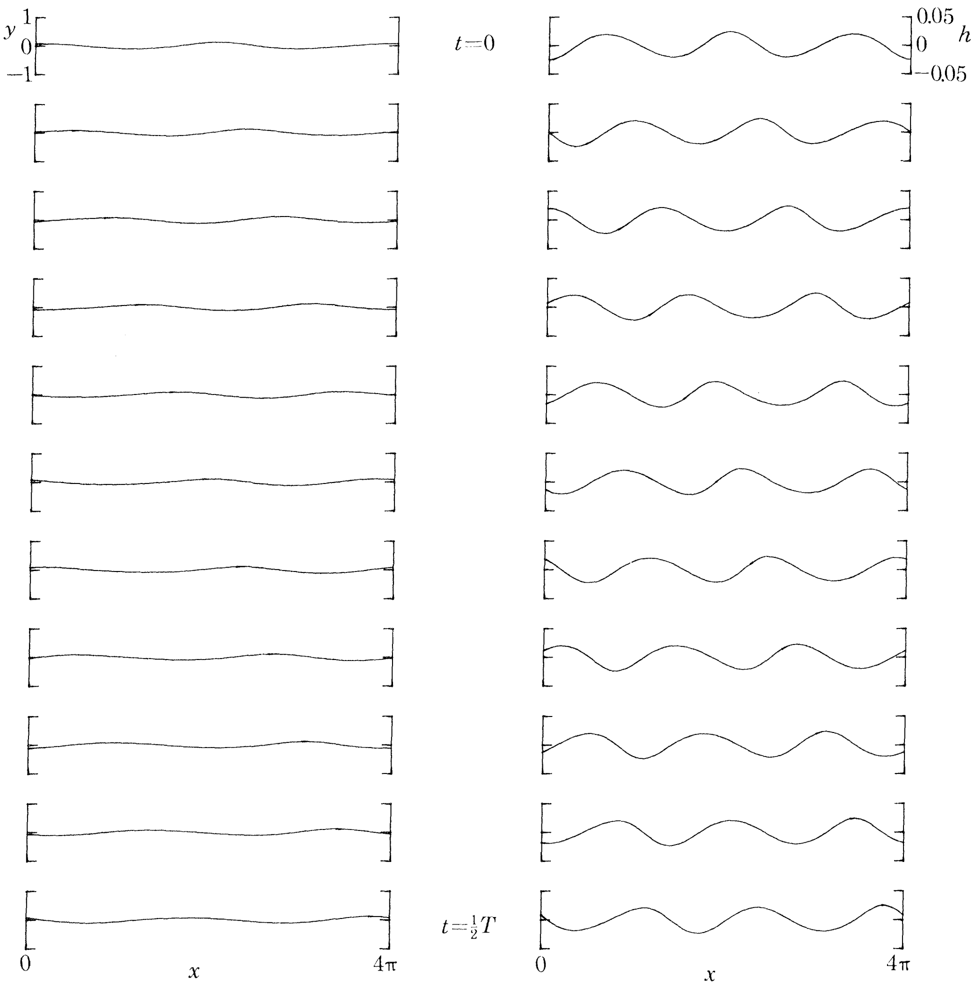

FIGURE 7. The mode $n = \frac{3}{2}$ when $ak = 0.10$ followed over one half-cycle of the perturbation.

we first compute the complete wave profile (unperturbed wave + perturbation), interpolate in time, interpolate in space, subtract the unperturbed wave, and then make the comparison to find C and R.

For $ak = 0.25$ theory predicts one growing mode $n = (\frac{1}{2}, \frac{3}{2})^+$ and one decaying mode $n = (\frac{1}{2}, \frac{3}{2})^-$, which indeed are found. The profiles for the growing mode are displayed in figure 10 in which the localized nature of the extrema are more apparent than before. The correlations at $t = \frac{1}{2}T$ still exceed 0.98 in magnitude. The growth-rates differ from those predicted by at most 5 %, with the decaying mode diminishing more slowly than predicted. This is not surprising since any numerical inaccuracies can feed energy to a potentially growing mode and so obscure the decaying one.

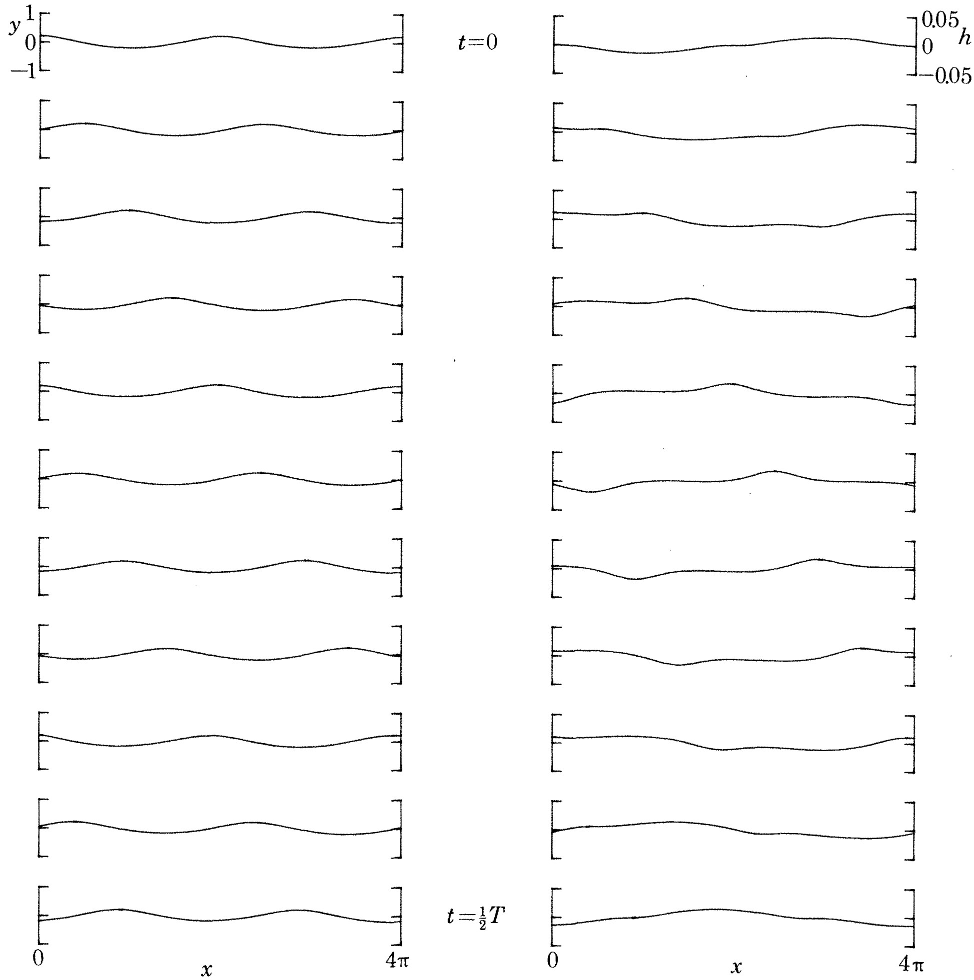

FIGURE 8. The mode $n = \frac{1}{2}$ when $ak = 0.20$ followed over one half-cycle of the perturbation. Compare figure 6.

The modes $(\frac{1}{2}, \frac{3}{2})^{\pm}$ at $ak = 0.32$ have already been discussed in § 3. $(\frac{1}{2}, \frac{3}{2})^{+}$ is of particular interest since it represents the fastest-growing Benjamin–Feir mode.

One of the unexpected results of the normal-mode theory is that a wave whose steepness is near $ak = 0.38$ will be stable to the modes $n = \frac{1}{2}$ and $n = \frac{3}{2}$. The results given in table 1 and plotted in figure 11 certainly suggest this. The correlation coefficient equals -0.994 for $n = \frac{1}{2}$, and there is a very slight decay in amplitude. We observe a lower correlation coefficient and an increased rate of decay from $n = \frac{3}{2}$. This is probably due to a variety of factors such as: (1) insufficiently converged eigenfunctions used as initial values, (2) the increased size of the perturbation amplitude for the mode $n = \frac{3}{2}$ due to the manner in which the eigenfunctions were normalized, and (3) inaccuracies in the time-stepping. Whatever the cause,

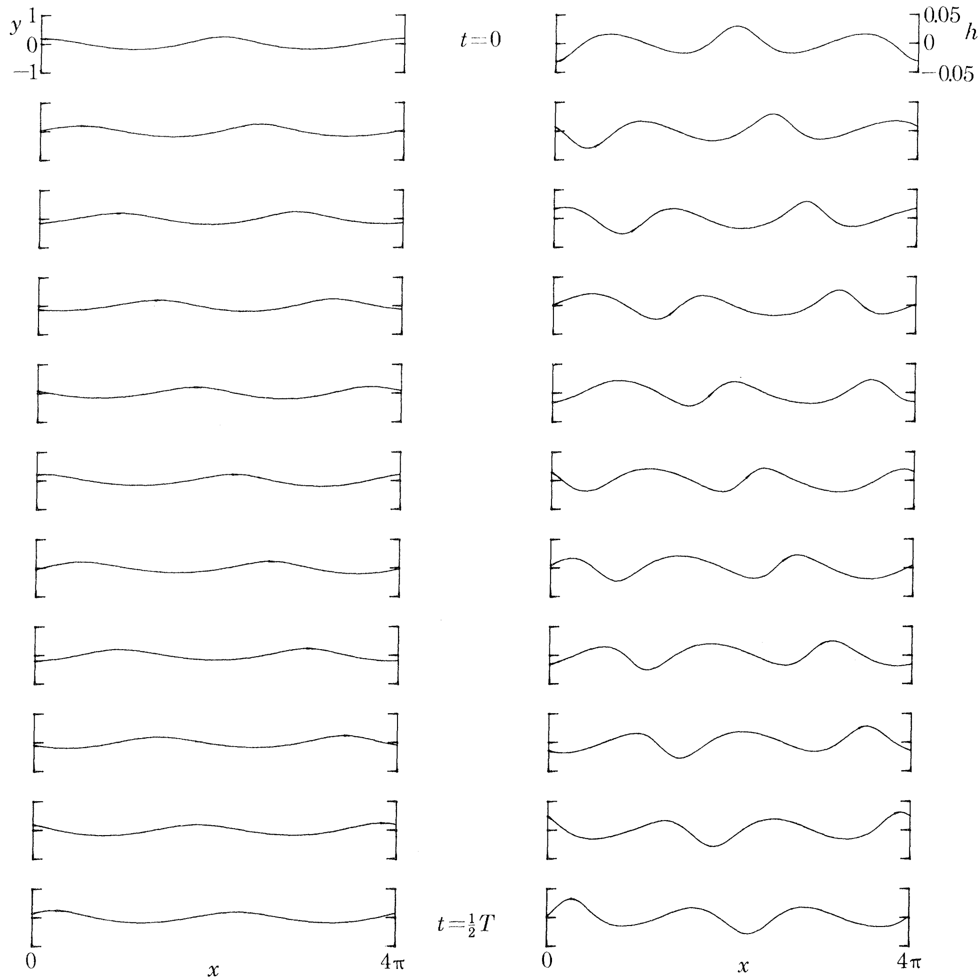

FIGURE 9. The mode $n = \frac{3}{4}$ when $ak = 0.20$ followed over one half-cycle of the perturbation. Compare figure 7.

the graph of C against t reveals a slightly noisy signal. The profiles for the two modes are shown in figures 11 and 12.

The normal-mode theory predicts that $ak = 0.40$ is just on the neutrally stable side of a very rapidly growing instability. We have tested the $n = \frac{1}{2}$ mode and have observed growth but at a rate significantly slower than that of the unstable waves on either side. This discrepancy is probably due to the factors mentioned previously and to the close proximity of the rapid-growth region. The profiles are shown in figure 13. One interesting feature of these is the near step-function shape of the perturbation at $t = 0$ and $t = \frac{1}{2}T = 17.07$. This is also apparent in the $n = \frac{1}{2}$ profiles for $ak = 0.38$ at $t = \frac{1}{4}T = 8.71$ as shown in figure 11. The perturbation elevates one wave trough and lowers the next. This also happens but to a lesser extent for

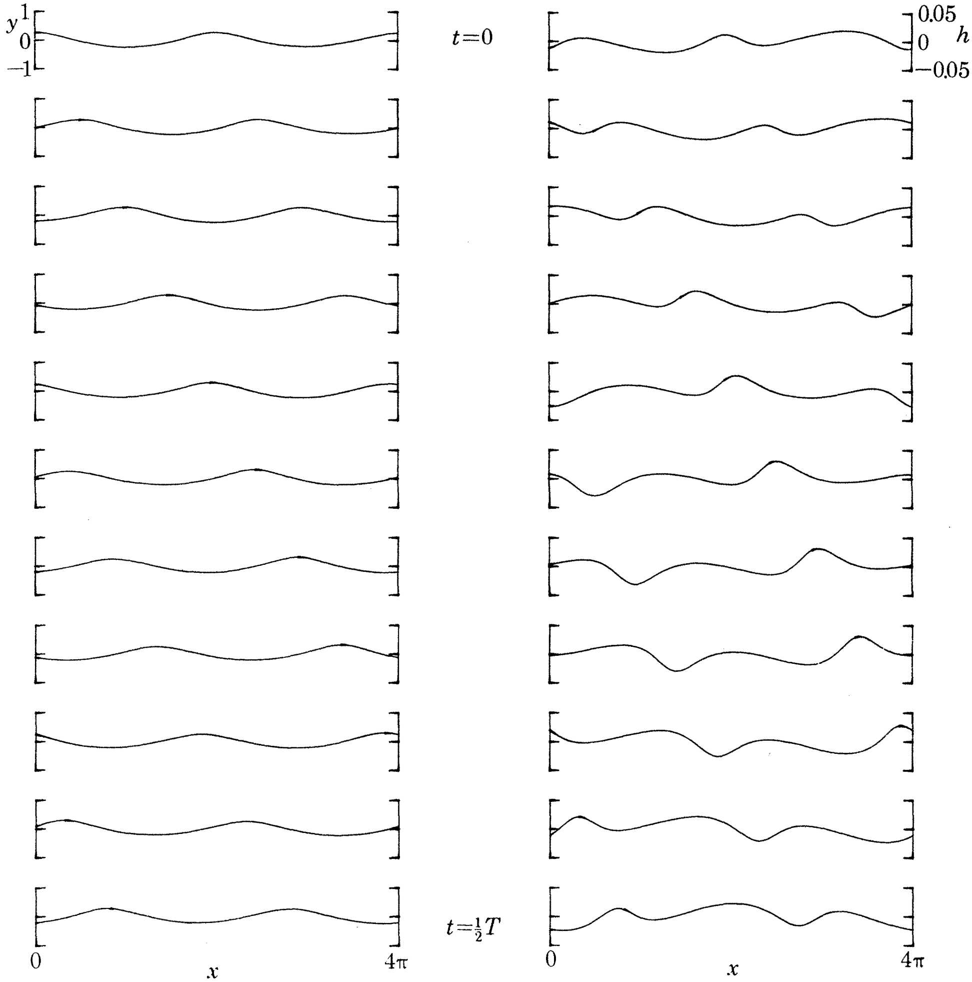

FIGURE 10. Development of the unstable mode $(\frac{1}{2}, \frac{3}{2})^{+}$ when $ak = 0.25$, over one half-cycle of the perturbation. The vertical scale on the right is enlarged times 20.

$n = \frac{3}{2}$, $ak = 0.38$ at $t = \frac{1}{4}T = 12.00$. We have not calculated the mode $n = \frac{3}{2}$ for $ak = 0.40$ because the relatively low frequency of the perturbation would have required an excessive amount of computer time, and the results would probably be too inaccurate to justify this.

The instability at $ak = 0.41$ differs from the others considered in two ways: (1) it has zero frequency with respect to the unperturbed waves (i.e. it remains 'locked on' to the crest) and (2) it grows very much more rapidly. The first fact means that we can measure its growth-rate at every time-step, and the second means we need only follow the wave a short time before it breaks. The profiles (with a 5 : 1 vertical exaggeration of the perturbation) are plotted in figure 14 over a non-dimensional time of slightly more than 2 units. The nature of the perturbation is such as to

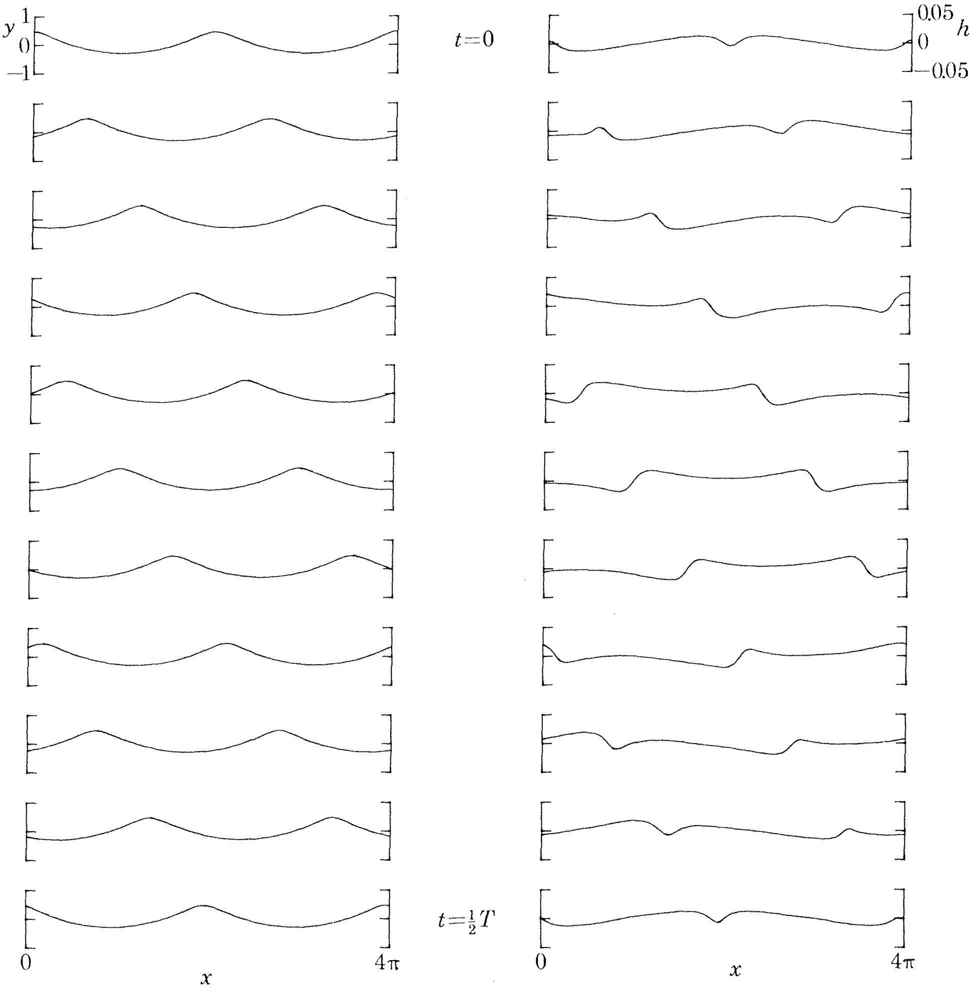

FIGURE 11. The neutrally stable mode $n = \frac{1}{2}$ when $ak = 0.38$ followed over one half-cycle of the perturbation. The vertical scale on the right is enlarged times 20.

reduce one wave crest and raise the other with not much alteration of the profile elsewhere. The crest-plots of figure 15 show the overturning. These computations were done with 120 points along the profile for increased resolution. The comparison of theoretical and observed growth-rates is given in figure 16, a plot of $\ln R$ against time. The spread of observed values at each data point represents the variability of R for slightly different methods of calculating the integrals. This gives a rough indication of the minimum size of the errors involved. The agreement with the linear theory is quite good especially during the initial stages of growth. At later times the deviations are not too great even when the perturbation has grown large enough to cause marked asymmetries in the wave profiles.

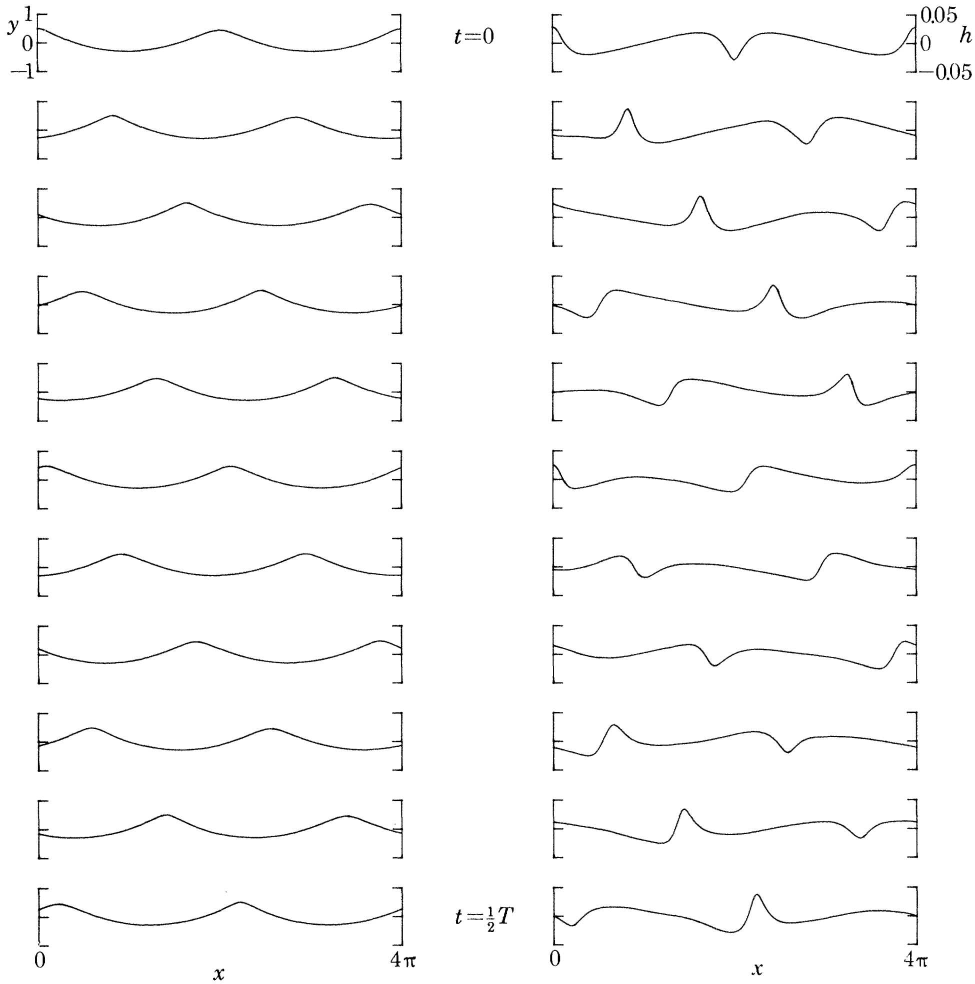

FIGURE 12. The neutrally stable mode $n = \frac{3}{2}$ when $ak = 0.38$; as in figure 11.

7. THE NONLINEAR STAGES OF GROWTH

Since the time-stepping method is not subject to any assumptions of linearity, we may use it to follow the later, nonlinear stages of the instabilities studied earlier. In figure 17 we show the mode $(\frac{1}{2}, \frac{3}{2})^+$ at $ak = 0.32$, carried through a second half-cycle $0.55\,T \leqslant t \leqslant 1.05\,T$. It will be seen that in the final stages every alternate crest ultimately steepens and breaks. Figure 18 shows a close-up of the crest in a frame of reference which is at rest relative to deep water. It will be seen how like the profiles are to those in figure 15. Indeed, the two figures are almost superposable.

It follows that when $ak = 0.32$ this instability, which began as a subharmonic of Benjamin–Feir type, later develops a different, local type of instability which is in

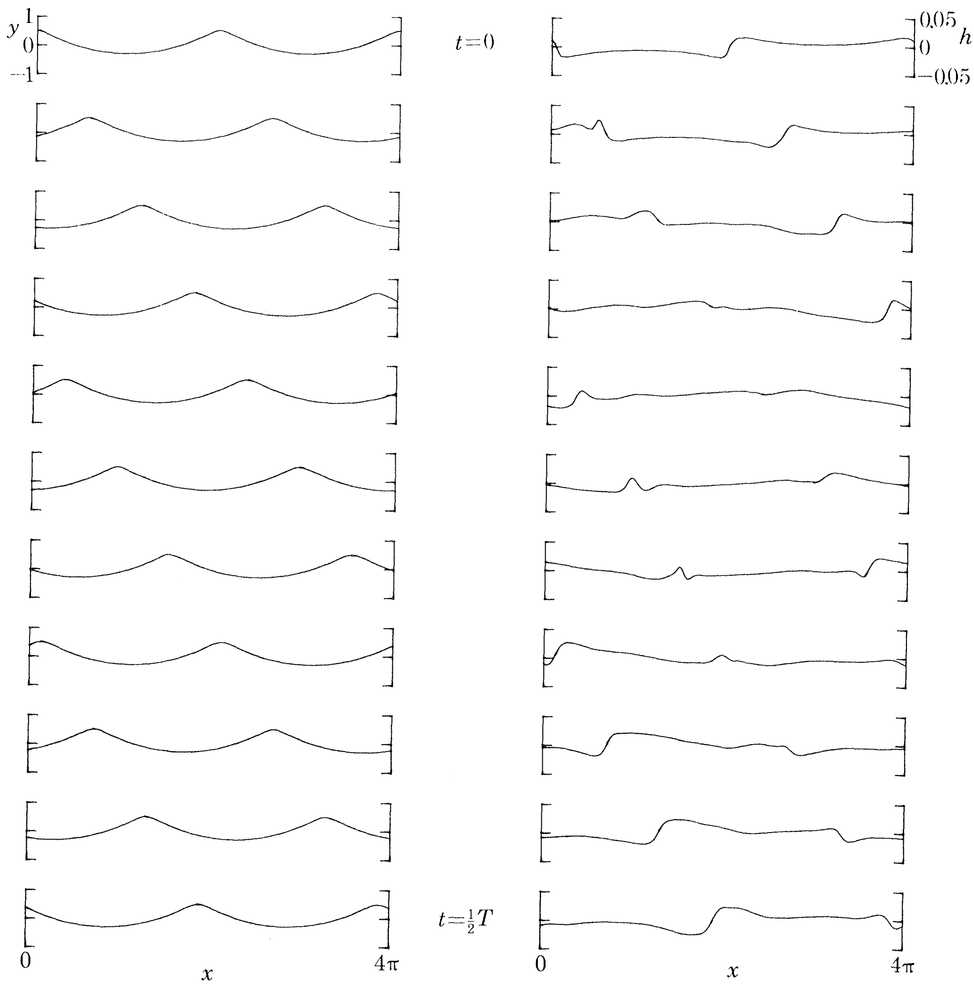

FIGURE 13. Development of the mode $n = \frac{1}{2}$ when $ak = 0.40$.

all respects similar to that arising at $ak = 0.41$. Since wave breaking involves energy loss, this leads to the disintegration of the original wave train.

To test whether the same phenomenon occurs with lower waves, a similar run was carried out on the mode $(\frac{1}{2}, \frac{3}{2})^+$ at the lower wave amplitude $ak = 0.25$. Figure 19 shows the surface profile, after nine successive half-periods. In the final profile the waves do indeed break (see also figure 20). A close-up of the breaking crest is shown in figure 21. Again, the close similarity to the local instability in figure 15 will be noted.

The calculated values of $C(ct, t)$ and β are shown in table 2. The constancy of β throughout the whole stage of development is indeed remarkable, as also is the closeness of β to the value 0.0132 derived from the independent normal-mode analysis.

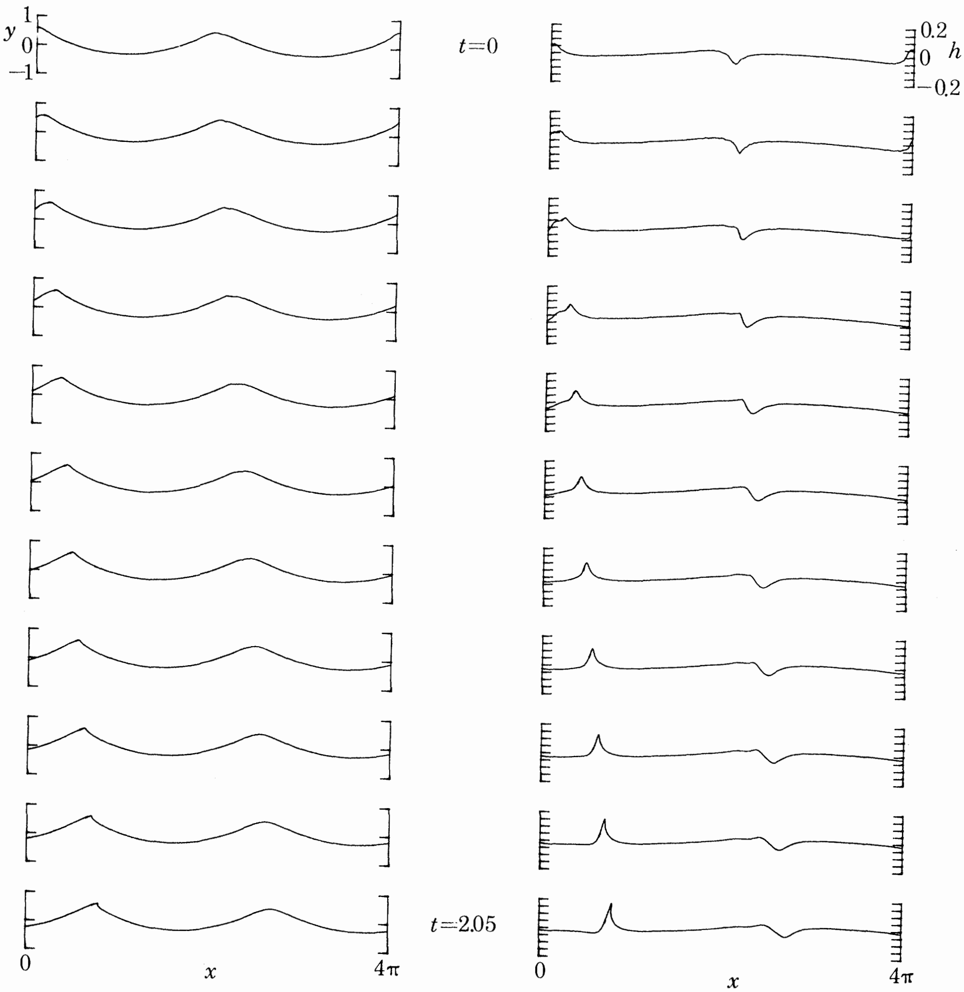

FIGURE 14. Development of the highly unstable mode $n = (\frac{3}{2})^+$ when $ak = 0.41$. The vertical scale on the right is magnified times 5.

Do all subharmonic instabilities lead to breaking? Because of the necessary machine time, the question cannot readily be answered by computation. One may reason as follows. It appears (from Longuet-Higgins 1978*b*) that an individual gravity wave becomes unstable when $ak \approx 0.436$. Roughly, then, one would expect an instability to lead to wave breaking if the local wave steepness exceeds this amount. If now we assume, first, that the subharmonic instability tends to increase the amplitude of every alternate wave but leave the wavelengths roughly unchanged, and secondly that the energy in each wave varies roughly as the square of the local amplitude, then we should expect subharmonics to lead to breaking only when

$$ak > 0.436/\sqrt{2} = 0.30.$$

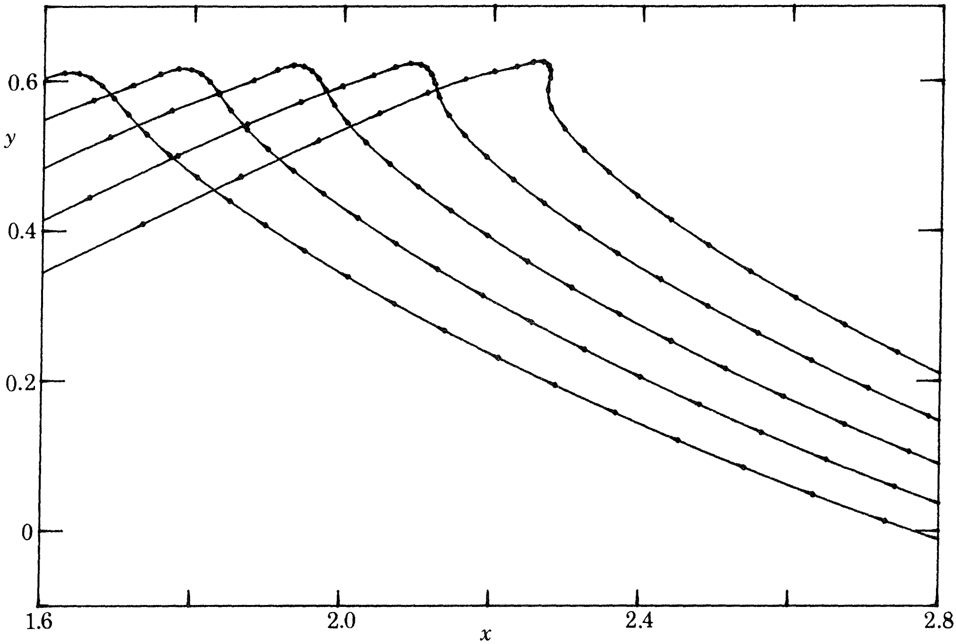

FIGURE 15. The mode $n = (\frac{3}{2})^{+}$ when $ak = 0.41$; enlargement of the wave crest, seen in a frame of reference at rest. Time interval between profiles is $2\pi/50$; the range, $1.37 \leqslant t \leqslant 1.87$.

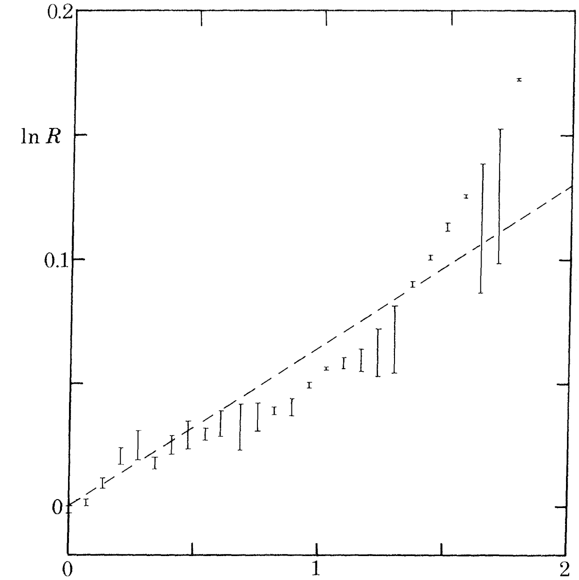

FIGURE 16. Growth of the mode $n = (\frac{3}{2})^{+}$ when $ak = 0.41$, shown by $\ln R(t)$ as a function of t. The broken line represents the growth βt where β is the rate corresponding to the normal-mode analysis.

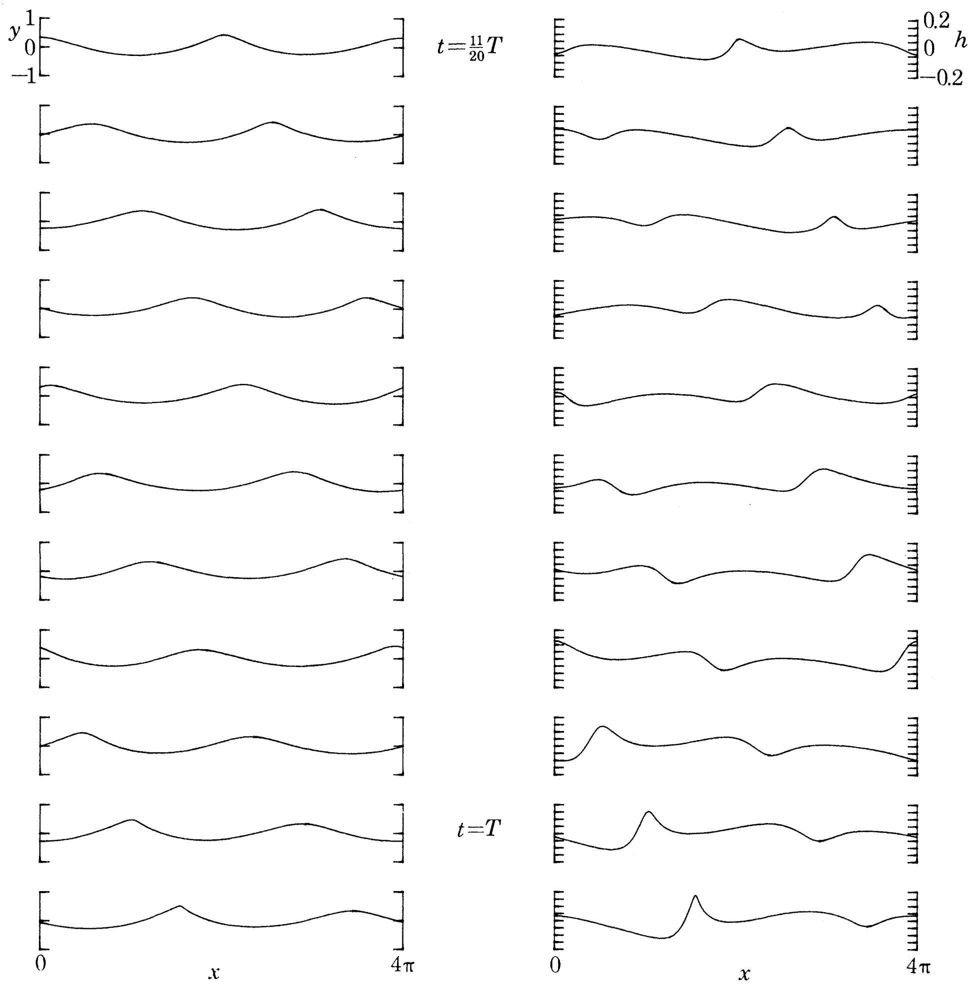

FIGURE 17. Later stages in the development of the mode $(\frac{1}{2}, \frac{3}{2})^+$ when $ak = 0.32$ (continuation of figure 1).

The example $ak = 0.25$ shows that this condition is contradicted. The reason appears to be that every alternate wave is not only increased in amplitude, but also *shortened* relative to its neighbours, so that locally a higher value of the wave steepness is attained.

This is confirmed by figure 22. In figure 22*a* is shown the variation with time of the individual wave amplitude a', defined as half the height of each crest above the trough in front of it. This is normalized by multiplying by the constant wavenumber k. The amplitude of each wave fluctuates, and the fluctuations grow in time. Figure 22*b* shows the individual wavenumber k' corresponding to the horizontal distance between adjacent troughs. This also fluctuates, by as much as 12 % in either direction, though these fluctuations are almost in quadrature with the fluctuations in a'.

Finally, figure 22c shows the fluctuations in the individual wave steepness $a'k'$. These are slightly greater than the fluctuations in $a'k$ above. The wave finally breaks when the individual wave steepness is about 0.39.

Hence it may be that waves of even lower amplitude than $ak = 0.25$ will develop instabilities ($m = 2$) to the point of breaking, assisted by a shortening of the individual wavelength.

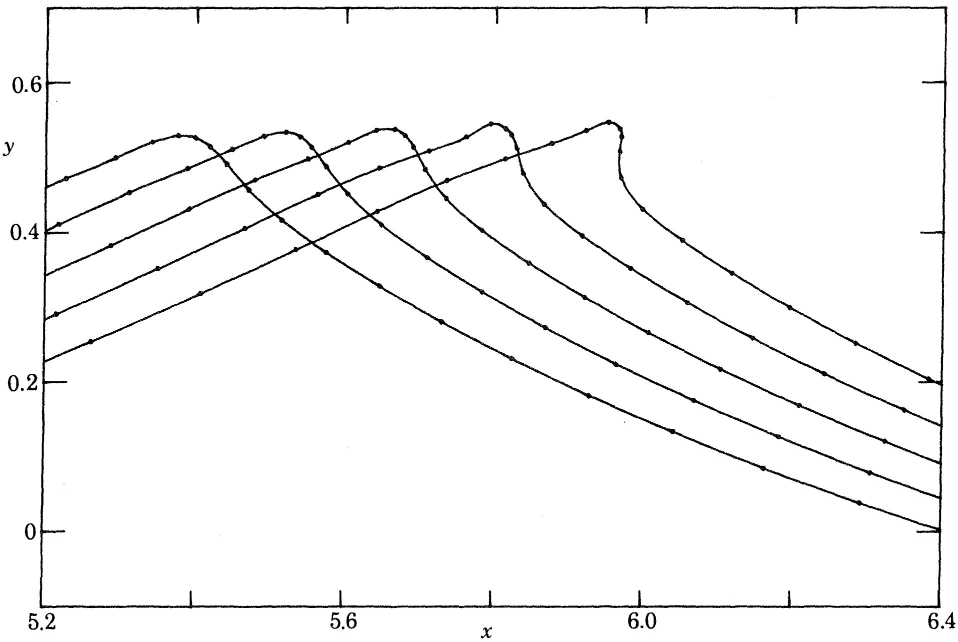

FIGURE 18. Enlargement of the wave crest in figure 20, near the instant of overturning, seen in a reference frame at rest. Time interval between profiles is $2\pi/50$; the range, $34.66 \leqslant t \leqslant 35.15$.

The profiles in figures 15, 18 and 21 are so similar as to suggest that the dynamics of the final stages of overturning are determined mainly by local conditions near the wave crest. If this is so then we would expect that the local length-scale l and time-scale τ would be related by

$$l/g\tau^2 = O(1),$$

where g denotes gravity. In fact if we take l to be the 'width' of the crest, measured by the horizontal distance over which the profile is convex, then $l \approx 0.4$ while the time τ for the evolution of the crest in figure 15 is above five plot intervals, i.e. about 0.6. Since $g = 1$ in these units the above relation is indeed satisfied.

However it will be noted that the time-scale for the *initial* growth-rate of the instability when $ak = 0.41$ is much longer than τ since β, though larger than for the Benjamin–Feir instabilities, is still only equal to 0.065. Thus β^{-1} is about 15.5.

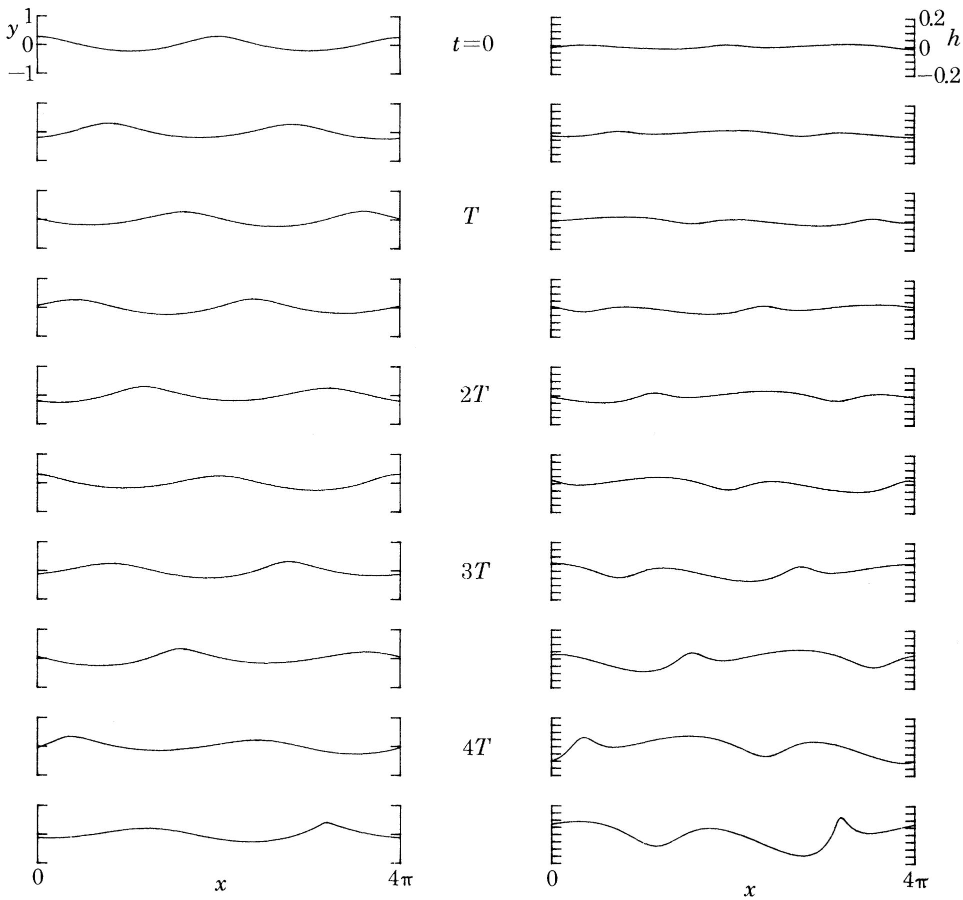

FIGURE 19. Later development of the unstable mode $(\frac{1}{2}, \frac{3}{2})^+$ when $ak = 0.25$. The profiles are seen at times $t = \frac{1}{2}sT$, $s = 0, 1, 2, \ldots, 9$ where T is the period of the mode.

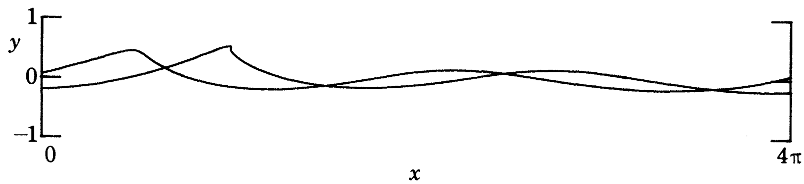

FIGURE 20. Profiles of the mode $(\frac{1}{2}, \frac{3}{2})^+$ near breaking, when $ak = 0.25$. The time interval between profiles is $2\pi/4$; $t = 140.86$ and 142.42.

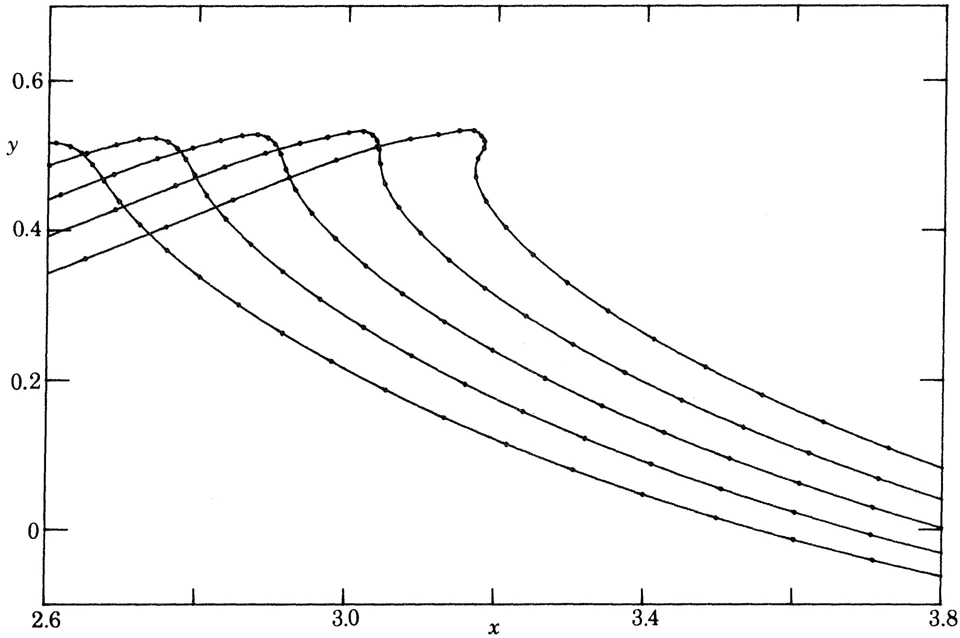

FIGURE 21. Enlargement of the overturning crests in the mode $(\frac{1}{2}, \frac{3}{2})^+$ when $ak = 0.25$, seen in a reference-frame at rest. Time interval between profiles is $2\pi/50$; the range, $141.92 \leqslant t \leqslant 142.42$.

TABLE 2. OVERALL GROWTH-RATE OF THE INSTABILITY $(\frac{1}{2}, \frac{3}{2})^+$ WHEN $ak = 0.25$

t	$C(ct, t)$	$\beta' = t^{-1} \ln R$
$\frac{1}{2}T = 14.61$	-0.992	0.0135
T	0.979	0.0134
$\frac{3}{2}T$	-0.982	0.0131
$2T$	0.965	0.0134
$\frac{5}{2}T$	-0.963	0.0133
$3T$	0.946	0.0133
$\frac{7}{2}T$	-0.915	0.0135
$4T$	0.863	0.0136
$\frac{9}{2}T$	-0.765	0.0141

8. CONCLUSIONS

By applying the independent time-stepping method of paper I we have confirmed and extended the conclusions of recent studies (Longuet-Higgins 1978*b*, *c*) relating to the stability of gravity waves. The initial rate of growth of each type of instability has been verified, and it is confirmed that subharmonic instabilities of Benjamin–Feir type are indeed confined to a certain range of wave steepnesses. Beyond this range, the perturbations are neutrally stable, until at about $ak = 0.41$ a second type of instability is found which leads directly to wave breaking.

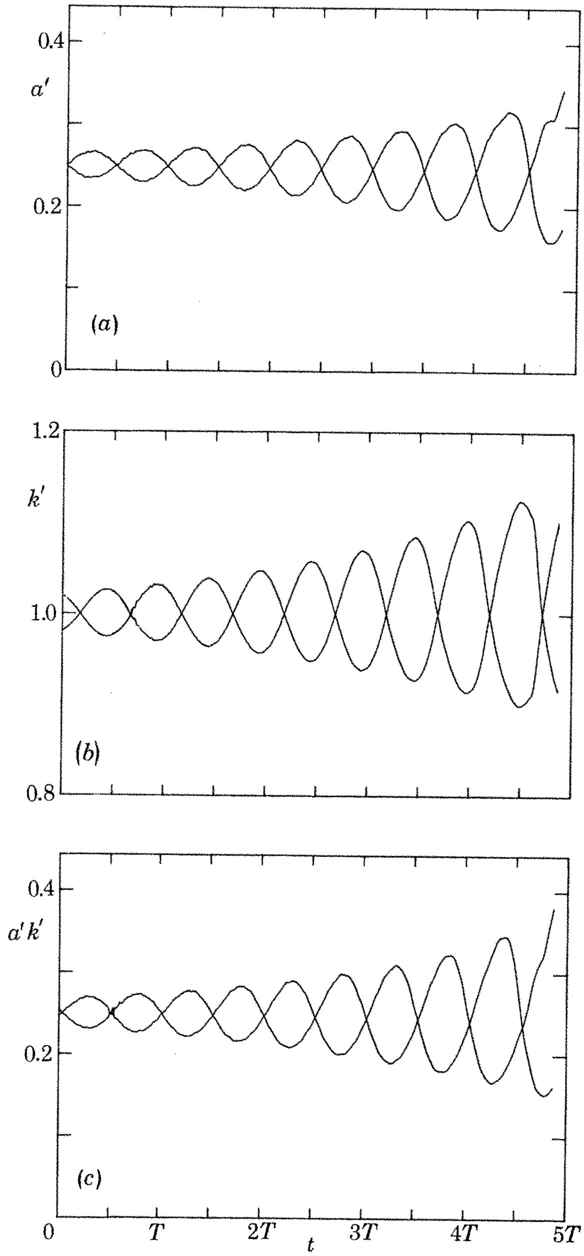

FIGURE 22. Time-dependence of local properties of the surface: (*a*) the local wave amplitude a'; (*b*) the local wavenumber k'; (*c*) the local wave steepness $a'k'$.

In the cases we have tested, the subharmonic instabilities apparently grow to the point where the wave crests develop local instabilities which again lead to breaking. The final stages of these breaking waves appear to be very similar in all cases, and their dynamics are related to local scales of length and time. This gives hope for a nonlinear theory of the latter stages of wave breaking.

As emphasized in earlier papers, the present calculations assume potential flow and neglect the possible influences of viscosity and capillarity, which must introduce qualitatively new effects. Moreover the motion is assumed to be two-dimensional, and the depth of water to be infinite. For sufficiently large-scale waves, viscosity and capillarity may indeed be negligible. The possible effects of three-dimensionality and of finite depth are, however, very interesting in the appropriate circumstances, and require further study.

Throughout this investigation we received support from the Departments of Energy and Industry, through a contract with the Institute of Oceanographic Sciences.

References

Benjamin, T. B. 1967 Instability of periodic wavetrains in nonlinear dispersive systems. *Proc. R. Soc. Lond.* A **299**, 59–67.

Cokelet, E. D. 1977 Breaking waves. *Nature, Lond.* **267**, 769–774.

Lighthill, M. J. 1967 Some special cases treated by the Whitham theory. *Proc. R. Soc. Lond.* A **299**, 28–53.

Longuet-Higgins, M. S. 1978*a* Some new relations between Stokes's coefficients in the theory of gravity waves. *J. Inst. Math. Appl.* (in the press).

Longuet-Higgins, M. S. 1978*b* The instabilities of gravity waves on deep water. I. Superharmonics. *Proc. R. Soc. Lond.* A **360**, 471–488.

Longuet-Higgins, M. S. 1978*c* The instabilities of gravity waves on deep water. II. Subharmonics. *Proc. R. Soc. Lond.* A **360**, 489–505.

Longuet-Higgins, M. S. & Cokelet, E. D. 1976 The deformation of steep surface waves on water. I. A numerical method of computation. *Proc. R. Soc. Lond.* A **350**, 1–26.